

# Bone Response to Free-Form Fabricated Hydroxyapatite and Zirconia Scaffolds: A Transmission Electron Microscopy Study in the Human Maxilla

Kathryn Grandfield, PhD student;\* Anders Palmquist, PhD;† Fredric Ericson, PhD;‡ Johan Malmström, PhD;§ Lena Emanuelsson, Tech;|| Christer Slotte, DDS, PhD;¶ Erik Adolfsson, PhD;# Gianluigi A. Botton, PhD;\*\* Peter Thomsen, MD, PhD;†† Håkan Engqvist, PhD‡‡

---

## ABSTRACT

**Background:** Understanding the interfacial reactions to synthetic bone regenerative scaffolds in vivo is fundamental for improving osseointegration and osteogenesis. Using transmission electron microscopy, it is possible to study the biological response of hydroxyapatite (HA) and zirconia (ZrO<sub>2</sub>) scaffolds at the nanometer scale.

**Purpose:** In this study, the bone-bonding abilities of HA and ZrO<sub>2</sub> scaffolds produced by free-form fabrication were evaluated in the human maxilla at 3 months and 7 months.

**Materials and Methods:** HA and ZrO<sub>2</sub> scaffolds (ø: 3 mm) were implanted in the human maxilla, removed with surrounding bone, embedded in resin, and sectioned. A novel focused ion beam (FIB) sample preparation technique enabled the production of thin lamellae for study by scanning transmission electron microscopy.

**Results:** Interface regions were investigated using high-angle annular dark-field imaging and energy-dispersive X-ray spectroscopy analysis. Interfacial apatite layers of 80 nm and 50 nm thickness were noted in the 3- and 7-month HA samples, respectively, and bone growth was discovered in micropores up to 10 µm into the samples.

**Conclusions:** The absence of an interfacial layer in the ZrO<sub>2</sub> samples suggest the formation of a direct contact with bone, while HA, which bonds through an apatite layer, shows indications of resorption with increasing implantation time. This study demonstrates the potential of HA and ZrO<sub>2</sub> scaffolds for use as bone regenerative materials.

**KEY WORDS:** FIB, free-form fabrication, hydroxyapatite, scaffolds, TEM, zirconia

---

\*PhD student, Department of Engineering Sciences, The Ångström Laboratory, Uppsala University, Uppsala, Sweden, and Department of Materials Science & Engineering, McMaster University, Hamilton, ON, Canada; †postdoctor, Institute for Clinical Sciences, Department of Biomaterials, Sahlgrenska Academy at University of Gothenburg, Gothenburg, Sweden; ‡associate professor, Department of Engineering Sciences, The Ångström Laboratory, Uppsala University, Uppsala, Sweden; §Institute for Clinical Sciences, Department of Biomaterials, Sahlgrenska Academy at University of Gothenburg, Gothenburg, Sweden; ||biomedical scientist, Institute for Clinical Sciences, Department of Biomaterials, Sahlgrenska Academy at University of Gothenburg, Gothenburg, Sweden; ¶Institute for Clinical Sciences, Department of Biomaterials, Sahlgrenska Academy at University of Gothenburg, Gothenburg, Sweden, and Department of Periodontology, The Institute for Postgraduate Dental Education, Jönköping, Sweden; #materials researcher, Swedish Ceramic Institute, IVE, Mölndal, Sweden; \*\*professor, Department of Materials Science & Engineering, McMaster University, Hamilton, ON, Canada; ††professor, Institute for Clinical Sciences, Department of Biomaterials, Sahlgrenska Academy at University of Gothenburg, Gothenburg, Sweden; ‡‡professor, Department of Engineering Sciences, The Ångström Laboratory, Uppsala University, Uppsala, Sweden

## INTRODUCTION

Implant design and interfacial stability remain important concerns for improving the biocompatibility of bone-graft substitutes. While a number of biological and synthetic alternatives for bone augmentation and regeneration exist, they do not come without their share of disadvantages and imperfections.<sup>1</sup> Potential drawbacks include donor-site infection and increased morbidity with use of autografts, for example.<sup>2</sup> There is a distinct need for improvement of synthetic materials for

---

Reprint requests: Ms. Kathryn Grandfield, Department of Engineering Sciences, Box 534, 751 21, Uppsala, Sweden; e-mail: kathryn.grandfield@angstrom.uu.se

© 2010 Wiley Periodicals, Inc.

DOI 10.1111/j.1708-8208.2009.00270.x

bone-graft substitutes and a deeper understanding of their interfacial interactions with the human body.

Hydroxyapatite (HA), on the one hand, has been at the forefront of biomaterials research over the last 30 years because of its bioactive nature. Composed of  $\text{Ca}_{10}(\text{PO}_4)_6(\text{OH})_2$ , bioactivity is often attributed to its structural and chemical resemblance to the inorganic constituent of bone. The proposed mechanism for bone bonding is a dissolution–reprecipitation process to form a biologically active apatite layer on the HA surface.<sup>3,4</sup> A most versatile biomaterial, non-load-bearing applications for HA range from coatings to cements, and to scaffolds.

Zirconia ( $\text{ZrO}_2$ ), on the other hand, while not a bioactive material, has considerable widespread use in the biomaterials field. Its chemical inertness combined with its strength have made it ideal for dental and load-bearing applications. Stable anchorage of  $\text{ZrO}_2$  implants requires a direct contact between implant and bone, and has been demonstrated in the rabbit model.<sup>5,6</sup>

In addition to materials selection, complete osseointegration depends on a number of factors including implant design. Pore morphology and interconnectivity are known to greatly influence bone ingrowth in bone-graft substitutes. It has been cited that interconnected macroporosity  $>100\ \mu\text{m}$  is necessary for vascularization associated with osteogenesis.<sup>7–9</sup> In addition, microporosity plays an important role in improving biocompatibility.<sup>7</sup>

While conventional casting techniques constrain implant shape and design, recent developments in computer-assisted design (CAD) and rapid prototyping methods, such as free-form fabrication, provide a feasible solution.<sup>10,11</sup> Free-form fabrication, which employs a three-dimensional ink-jet printing principle, is an effective method to control pore architecture (size, shape, and interconnectivity) and tailor scaffolds for specific clinical applications.

Particularly for the structural and interfacial characterization of bone growth around such implants, preparation of biomaterial–bone interfaces is a major challenge. Because of the differences in mechanical strength of the adjacent materials, conventional transmission electron microscopy (TEM) preparation by ultramicrotomy results in a variety of artifacts. Problems related to delamination of interfaces, plastic deformation of soft materials, fracture of brittle materials, and limitations in specimen thinness have been reported

to constrict the acquisition of elemental and high-resolution data.<sup>12,13</sup> Focused ion beam (FIB) preparation eliminates the artifacts associated with ultramicrotomy and has been used for all sample preparations in this study.

Previously, it has been shown in a rabbit *in vivo* model that free-form fabricated HA scaffolds bond to bone through an interfacial apatite layer, while  $\text{ZrO}_2$  scaffolds form a direct contact to bone.<sup>6</sup> The role of microporosity on bone response has also been demonstrated to promote increased bone ingrowth and bone contact.<sup>14</sup> In this study, TEM and analytical techniques enabled the evaluation of microporous HA and  $\text{ZrO}_2$  scaffold–tissue interfaces at the nanometer scale in a human *in vivo* model.

## MATERIALS AND METHODS

### Materials

Porous HA and  $\text{ZrO}_2$  scaffolds ( $\phi = 3\ \text{mm}$  and  $l = 4\ \text{mm}$ ) were created by free-form fabrication. Square-shaped interconnected channels (approximately  $350\ \mu\text{m}$ ) define the macroporous structure that was created using a CAD tool (Solid Works, Concord, MA, USA) (Figure 1). The mold structure was formed from thermoplastic building material (Proto build, Sanders Prototype Inc., Milton, NH, USA) and supported by a wax-based surround (Proto support, Sanders Prototype Inc.). Free-form

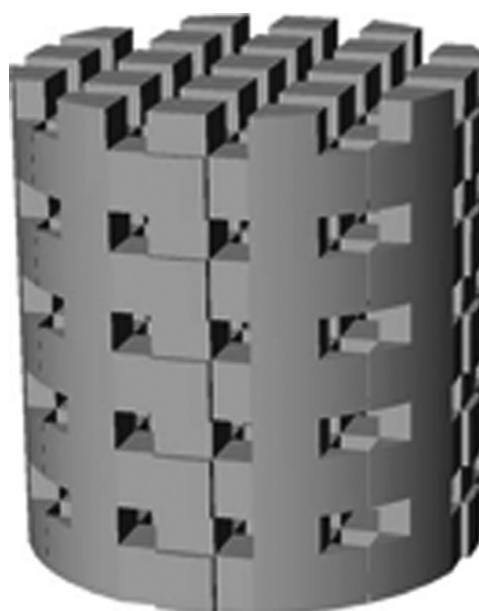


**Figure 1** Computer-assisted design graphic of the scaffold geometry showing interconnected square-shaped pore channels.

fabrication equipment (Model Maker II®, Sanders Prototype Inc.) using an ink-jet printing method, with a layer thickness of 50 μm, was used to create the molds. Ceramic suspensions of HA (Plasma Biotol Ltd., Tideswell, Buxton, UK) and ZrO<sub>2</sub> (Tosoh Corp., Tokyo, Japan) prepared by ball milling were loaded into the molds 48 vol% and 50 vol%, respectively. The addition of a binder (LDM7651S, Clariant AB, Göteborg, Sweden) enabled the variation of interconnected microporosity and improved green strength of the HA scaffold. Slip casting on a plate of plaster was used to remove excess water. The cast materials were heated at a rate of 1°C/min up to 600°C to burn away the mold and additives. Further heating of 5°C/min up to 1,200°C for HA and 1,500°C for ZrO<sub>2</sub>, holding of the temperature for 2 hours, and then decreasing by 5°C/min produced the sintered scaffolds.

Fabricated HA scaffolds contain 22.3 vol% microporosity (22.1 vol% open and 0.2 vol% closed), and ZrO<sub>2</sub> scaffolds contain 0.7 vol% closed porosity, measured by Archimedes' principle. The square-shaped interconnected pore channels contribute to 40 vol% macroporosity.

The phases present in the ZrO<sub>2</sub> and HA scaffolds were analyzed by X-ray diffraction (XRD) using a Guinier-Hägg camera and CuK $\alpha$  radiation. Grain size of the scaffold material was determined using TEM.

## Subjects and Surgical Procedure

Patients recommended for implant treatment in the pre-molar region of the maxilla and between the ages of 20 years and 75 years were included in this study. Exclusion criteria consist of a clinical history of smoking (>5 times per day), immunosuppressive agents, recent cardiovascular disease, cardiovascular/renovascular drugs, hormonal disease, radiotherapy in the head/neck region, and infection. Ethical approval for this study was obtained from the ethical research committee at Linköping University, Linköping, Sweden (Dnr. M35-05).

Twelve patients (six men and six women, 48–72 years old) received the implants in the maxilla. Anesthesia (10–12 mL, Xylocaine Dental Adrenalin® 2%, 12.5 μg/mL, Dentsply, Skarpnäck, Sweden) was administered locally. Twist drills with a diameter of 3 mm were used to prepare holes 4 mm deep under profuse irrigation with saline (NaCl 9 mg/mg, ACO, Upplands Väsby,

Sweden). Scaffolds were press fit into the holes, rinsed with saline, and mucoperiosteal flaps were sutured with Vicryl® 5-0 (Johnson & Johnson, Sollentuna, Sweden). Postoperatively, patients received analgetics (Diclofenac T ratiopharm 50 mg, ratiopharm AB, Helsingborg, Sweden, three times daily for 1–2 days). Antibiotics (phenoxymethyl penicillin 4 g daily or clindamycin 600 mg daily) were prescribed for 7 days. Patients were advised to rinse with a 0.1% chlorhexidine digluconate solution (Hexident, Ipex, Solna, Sweden) daily for 2 weeks postoperatively.

## Retrieval and Specimen Processing

Specimens were retrieved with surrounding bone tissue using a trephine drill (5 mm inner diameter). Retrieved specimens were fixed by immersion in glutaraldehyde (2.5% in 0.05 M sodium cacodylate buffer, pH 7.4) and dehydrated in ethanol. Undecalcified specimens were embedded in plastic resin (LR White, the London Resin Co. Ltd., Hampshire, UK). Sawing divided specimens in half longitudinally (Exakt cutting and grinding equipment, Exakt Apparatebau, Norderstedt, Germany).<sup>15</sup> Surfaces were polished and sputter coated with 10 nm of gold for scanning electron microscopy (SEM) analysis. While 12 patients initially took part in the investigation, only four blocs were allotted for SEM and TEM analysis, while the remainders were intended for another study.

## Analysis

Preliminary SEM investigation was performed with a JEOL 7000F FEG SEM (JEOL Ltd., Akishima, Tokyo, Japan) operated at an acceleration voltage of 15 kV. SEM analysis with backscattered electrons enabled the identification and quantification of bone-scaffold contact.

Samples for TEM study were prepared by a novel FIB technique and in situ lift-out method.<sup>16</sup> A Zeiss NVision 40 dual-beam FIB (Carl Zeiss AG, Oberkochen, Germany) equipped with a 30 kV gallium ion column, FEG SEM, carbon gas injector system, and Kleindiek probe drive system was used. The preparation technique is depicted in Figure 2. Areas of apparent bone-implant contact were selected for preparation. A layer of carbon, approximately 1 μm thick, was deposited in a rectangle 30 × 2 μm to protect the underlying surface from ion beam damage. Trapezoidal-shaped trenches were milled on either side of the carbon deposit to a depth of

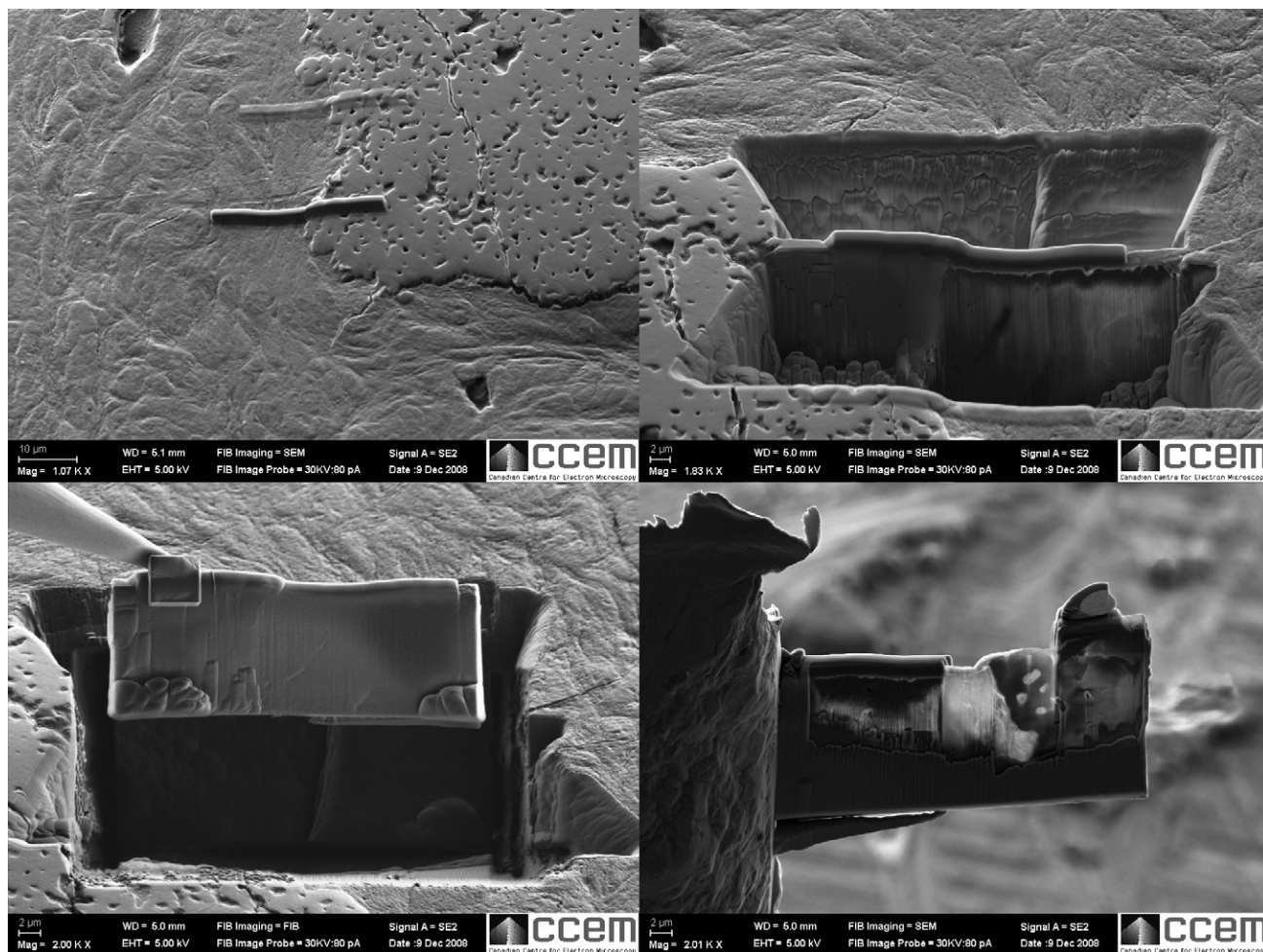


**Figure 2** The transmission electron microscopy sample preparation method using an in situ lift-out focused ion beam method.

approximately 11  $\mu\text{m}$  using a beam current of 30 nA. The resulting lamella was cut free underneath and on one side using a beam current of 6.5 nA. The tungsten lift-out probe was attached to the top of the lamella by carbon deposition. The final side of the lamella was cut free, and the sample was lifted out in situ. A TEM grid was inserted into the FIB chamber, and the lamella was attached to the side of the grid using C deposition. Finally, the sample was thinned to electron transparency using beam currents from 1.5 nA down to 40 pA.

TEM was performed on a FEI Titan 80-300 (S)TEM (FEI Co., Hillsboro, OR, USA) operated at 300 keV. Elemental maps and line profiles were collected using an Oxford energy dispersive X-ray spectroscopy (EDXS) detector and Inca software (Oxford Instruments, Oxford, UK) in scanning TEM mode. Images were obtained using a high-angle annular dark-field detector to enhance Z-contrast compared with bright-field imaging.<sup>17</sup>

## RESULTS

### Clinical Evaluation

All surgical sites healed uneventfully. Bone overgrowth was noted in a few samples.

### Material

XRD analysis, shown in a previous study,<sup>18</sup> confirmed the presence of mainly tetragonal  $\text{ZrO}_2$ , with small amounts transformed to monoclinic when the material was crushed during sample preparation. The HA scaffolds contained minor amounts of  $\beta$ -tricalcium phosphate ( $\beta$ -TCP). Grain size was measured in TEM to be approximately 1.2  $\mu\text{m}$  and 390 nm for HA and  $\text{ZrO}_2$  scaffolds, respectively (Figure 3). Drastic changes in grain size after implantation were not observed.

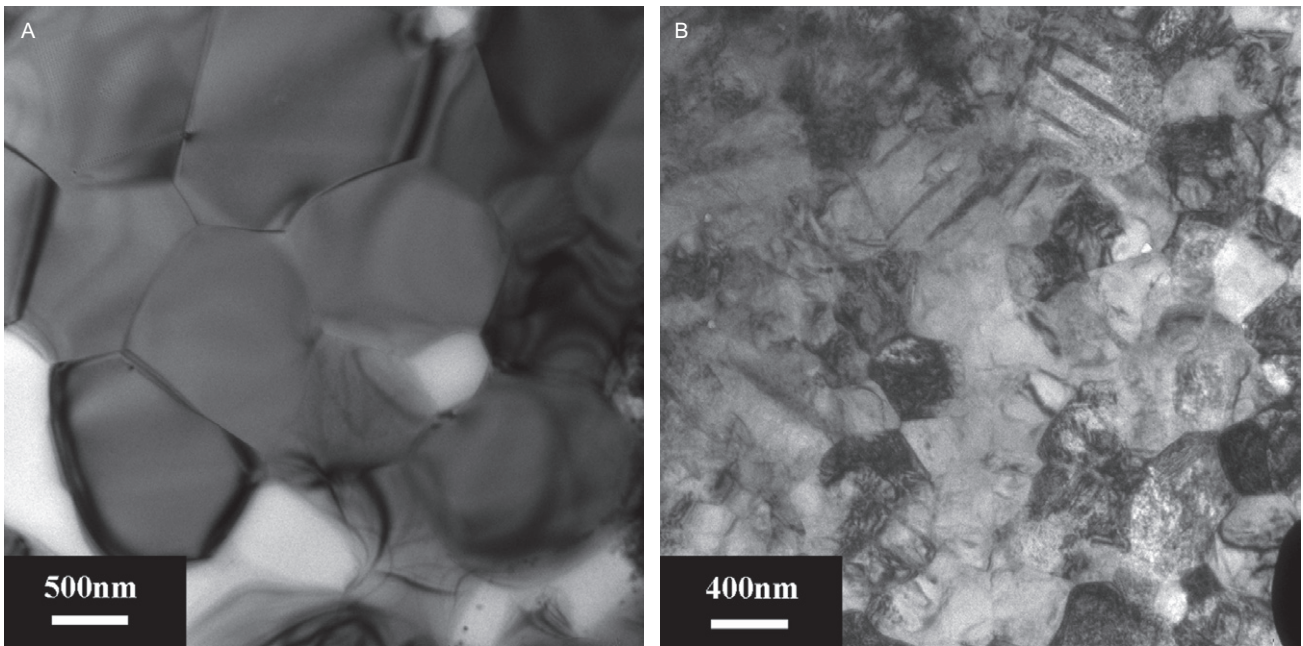


**Figure 3** Transmission electron microscopy image of the native (A) hydroxyapatite and (B) zirconia scaffolds prior to implantation.

### Light Microscopy and SEM

Light microscopy and SEM were performed in detail in a previous study.<sup>18</sup> Morphometry indicated a significantly higher bone area and bone-to-scaffold contact for HA scaffolds compared with ZrO<sub>2</sub>, and no presence of an intervening fibrous structure.<sup>18</sup> The scaffolds with bone ingrowth and regions selected for TEM sample preparation are shown in Figure 4.

### Scanning TEM

In HA scaffolds implanted for 3 months, images reveal the *in vivo* formation of an interfacial apatite layer that

exhibits intimate contact with bone along the interface region shown in Figure 5. According to the proposed *in vivo* mechanisms of HA dissolution–reprecipitation and a previous study in the rabbit model, it is expected that the interfacial apatite layer spans the entire surface. A similar apatite layer is noted in some regions in the 7-month sample. However, indications of apatite resorption and replacement with bone are denoted in Figure 6.

Evidence of effective bone ingrowth and implant fixation is further demonstrated by the detection of bone growth into micropores, seen in TEM (Figure 7) and confirmed by FIB cut and view (not shown), up to

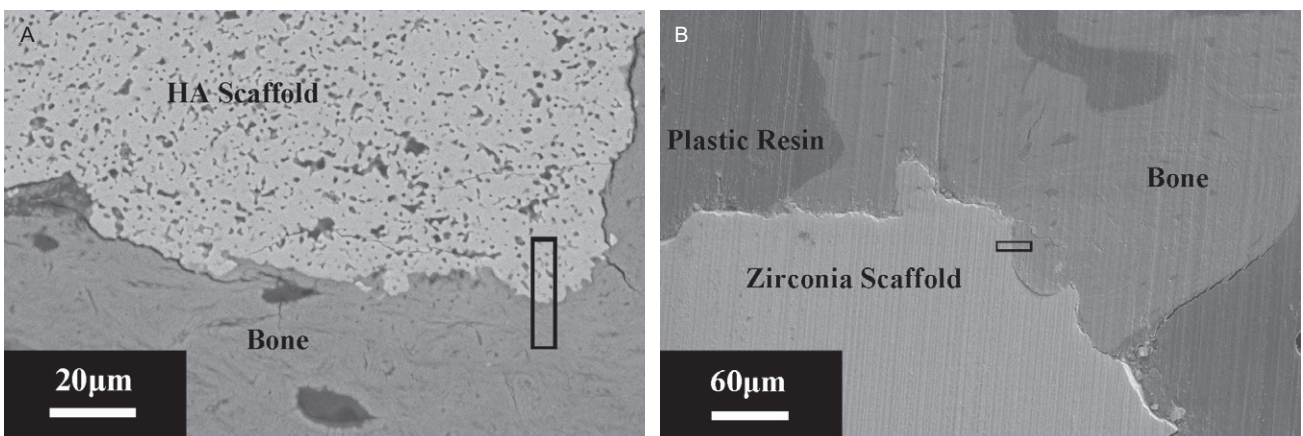


**Figure 4** Scanning electron micrographs of the embedded tissue blocks showing bone ingrowth in (A) hydroxyapatite (HA) and (B) zirconia scaffolds. Regions selected for focused ion beam transmission electron microscopy sample preparation are indicated by boxes.

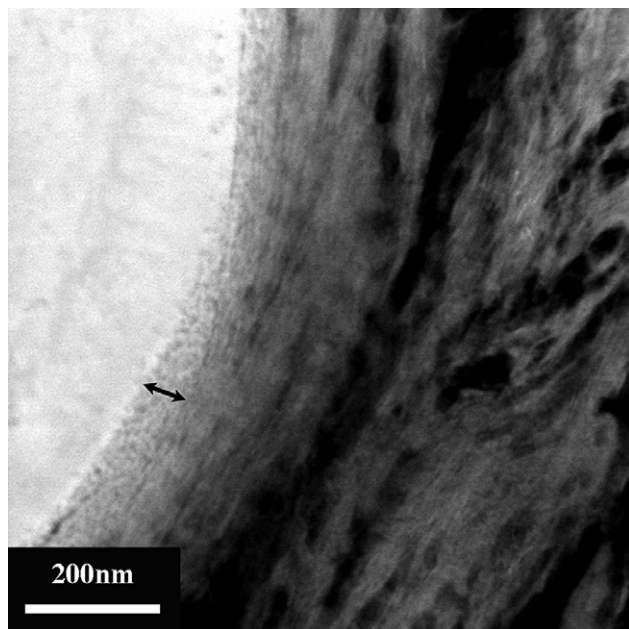


**Figure 5** High-angle annular dark-field scanning transmission electron microscopy image of the cortical bone–hydroxyapatite scaffold interface implanted for 3 months. An interfacial apatite layer 80 nm in thickness is indicated by the *arrow*. Collagen banding was observed perpendicular to the scaffold surface.

10  $\mu\text{m}$  from the surface in both HA samples. Compositional analysis on growth in micropores yields similar results to bone in bulk.

EDXS line scans across the HA scaffold–bone interface at 7 months reveal a composition gradient, confirming the existence of an interfacial apatite layer richer in Ca and P closer to the scaffold surface (Figure 8). The same line scans across the  $\text{ZrO}_2$  7-month sample yield a dramatic drop in Ca and increase in Zr content at the interface, confirming the absence of an interfacial apatite layer (Figure 9B). The absence of this layer is further supported by the image in Figure 9A. Lack of intimate bone–implant contact prevented the preparation of a  $\text{ZrO}_2$  sample at 3 months.

## DISCUSSION

Use of the FIB for sample preparation was critical for site-selective preparation and analysis of the scaffold–tissue interface. Precautions to avoid ion beam damage were taken, such as sequential reduction in ion beam current. FIB-induced damage is not suspected as structures resemble those in the literature prepared by FIB and other methods where the collagen banding is also observed.<sup>19,20</sup> Separation of bone from the scaffold interface, whether because of specimen retrieval or pro-

cessing, prevented high-resolution analysis of scaffold–bone interfaces for the  $\text{ZrO}_2$  sample at 3 months and inside the square-shaped macroporous channels for all samples.

The scaffolds were analyzed with a variety of electron microscopy techniques to determine their bone-bonding performance in vivo. HA samples at both 3 months and 7 months exhibit an interfacial apatite layer. The proposed mechanism for apatite formation on HA is a dissolution–reprecipitation sequence.<sup>4</sup> Apatite layers as thick as 1,000 nm have been reported,<sup>21</sup> and precipitation of crystallites have been observed in as little as 3 hours post-implantation.<sup>22</sup> In this investigation, layers of 80 nm and 50 nm thickness are reported. The absence of formation of a dense apatite layer for  $\text{ZrO}_2$  samples may be because of the inert chemical nature of the material.  $\text{ZrO}_2$ , known to be a bio-inert material, has limited interaction in the body.<sup>23</sup> Results for both materials are in agreement with surface response observed around the scaffolds implanted in rabbit tibia in a previous study.<sup>6</sup>

The addition of microporosity to scaffold materials has been reported to enhance the bioactivity of bone substitutes.<sup>14,24</sup> These scaffolds, in particular, displayed increased bone ingrowth and bone contact with a

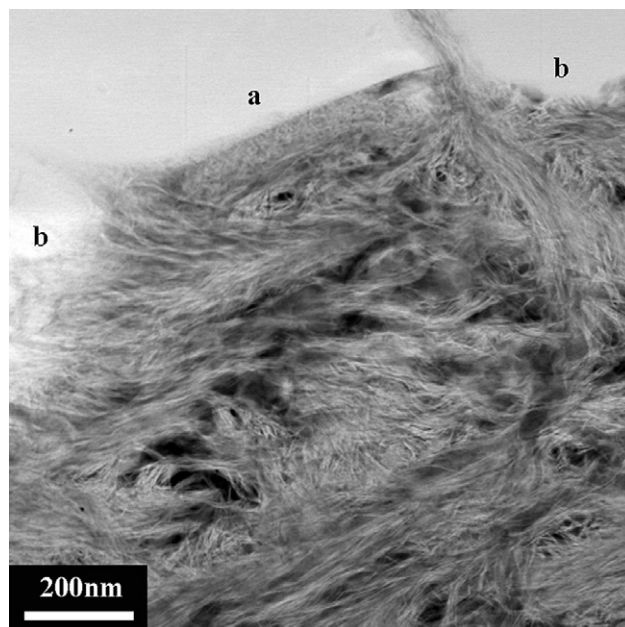


**Figure 6** High-angle annular dark-field scanning transmission electron microscopy image of the cortical bone–hydroxyapatite scaffold interface implanted for 7 months. “a” denotes an interfacial apatite layer 50 nm in thickness. “b” marks regions without an interfacial layer. Collagen banding with 67 nm periodicity is clear in the bulk bone and at the interface regions absent of interfacial apatite.

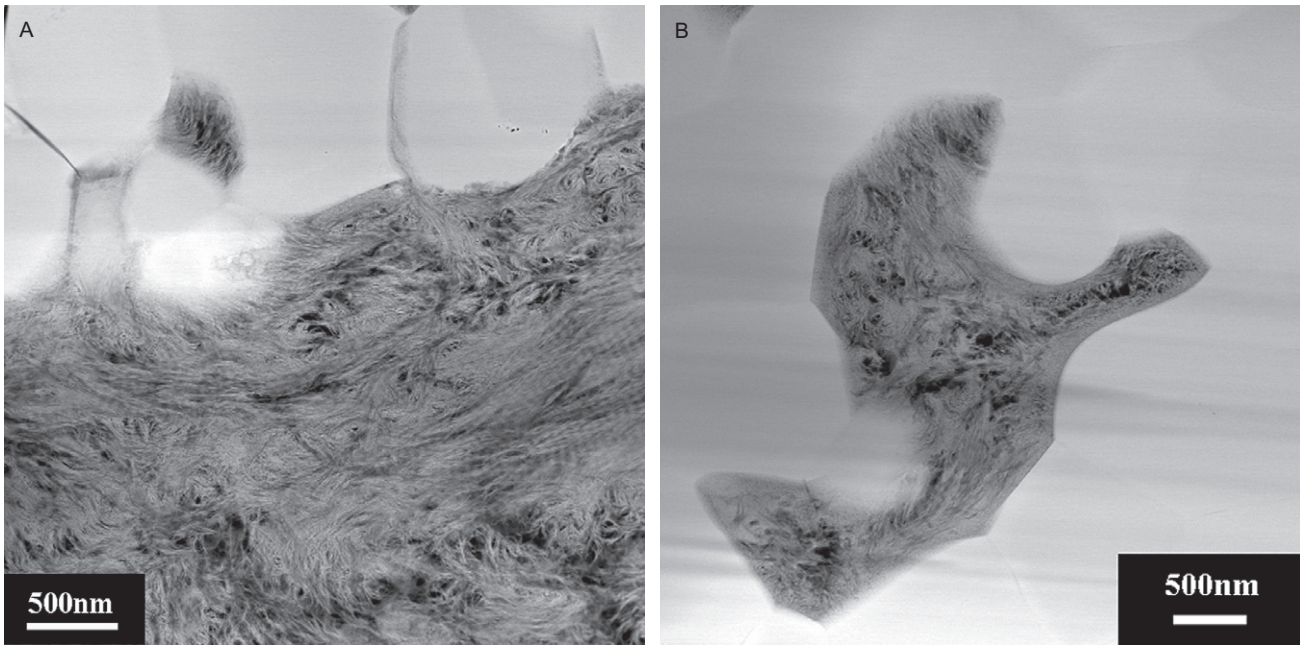


**Figure 7** High-angle annular dark-field scanning transmission electron microscopy image of the hydroxyapatite scaffold implanted for 7 months. Bone growth into the micropores is observed near the interface in (A), and further into the bulk in (B). Focused ion beam confirmed the growth into pores up to 10  $\mu\text{m}$  into the scaffold.

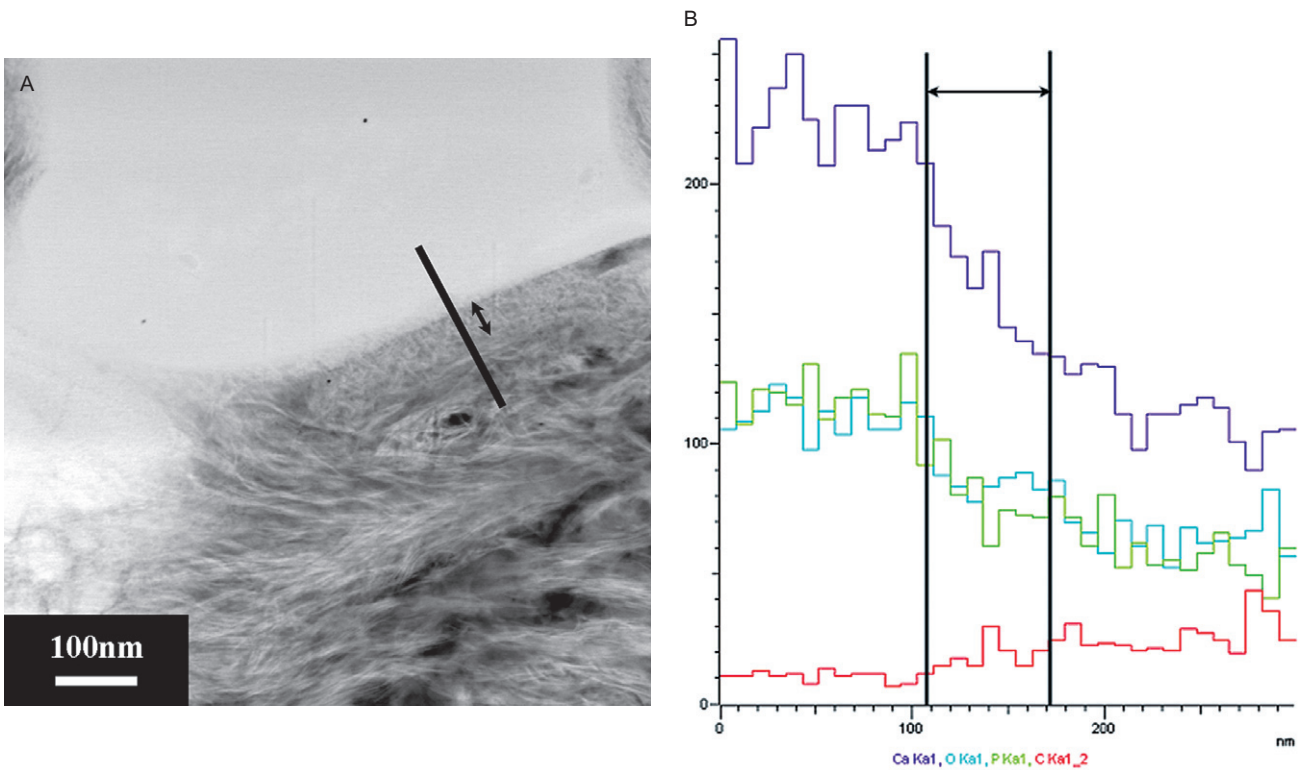


**Figure 8** High-angle annular dark-field scanning transmission electron microscopy image of the cortical bone–hydroxyapatite scaffold interface implanted for 7 months (A), and accompanying EDXS line scan profile (B) showing a gradual decrease in Ca and P, and increase in C concentrations across the interface, confirming the presence of an interfacial apatite layer.

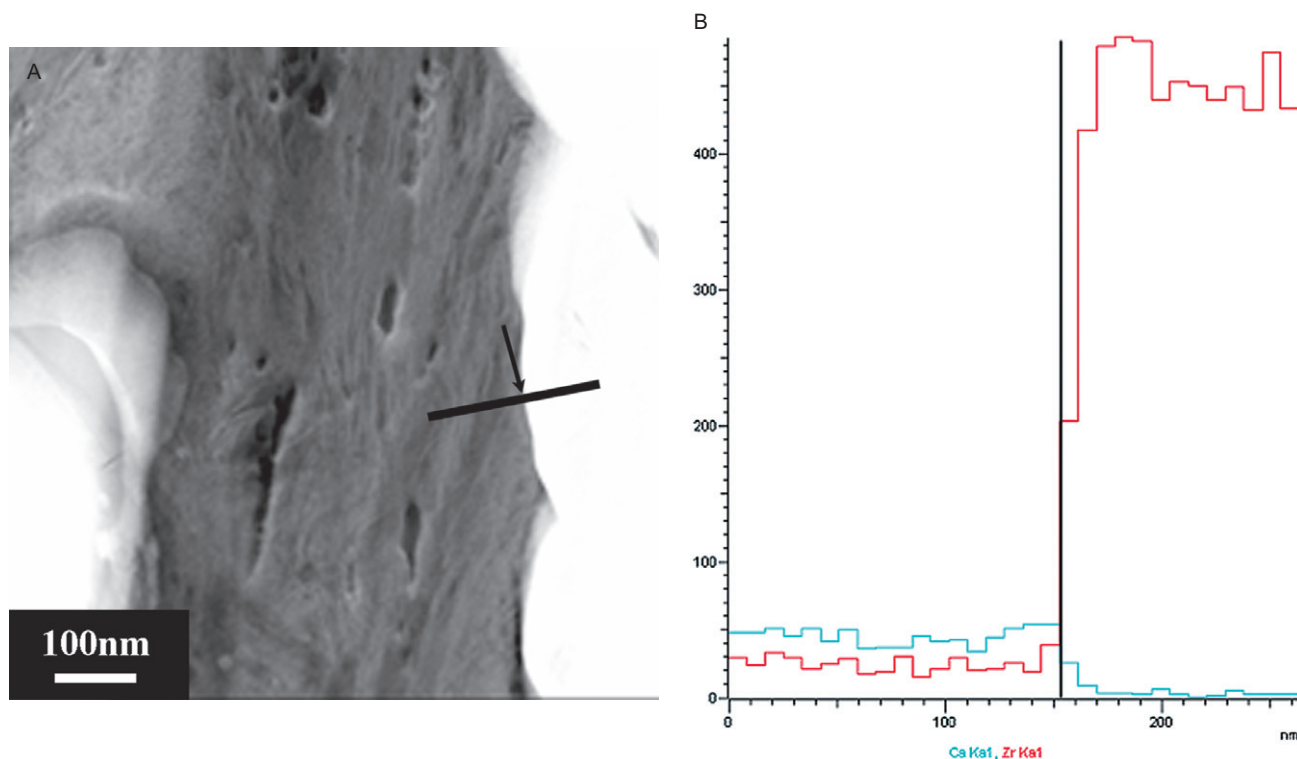


**Figure 9** High-angle annular dark-field scanning transmission electron microscopy image of the cortical bone–zirconia scaffold interface implanted for 7 months (A), and accompanying EDXS line scan profile (B) showing an abrupt drop in Ca concentration and increase in Zr concentration at the interface. The lack of concentration gradient over this interface indicates an absence of an interfacial apatite layer and confirms the direct bond of zirconia to bone.

microporous structure versus those fabricated without microporosity.<sup>14</sup> It is clear that the pores show an affinity for bone growth. Detection of bone in micropores demonstrates the open network of pores in the scaffolds and migration of bone-forming cells into the structure, which is essential for improving bioactive fixation of the implant. It is interesting to note the absence of an interfacial apatite layer and collagen-banding structure in HA detected in the micropores. Instead, the HA exhibits a fibril structure, which was also seen in the rabbit model.<sup>6</sup> Bone growth located at the exterior-implant interface exhibits the standard 67 nm banding periodicity typical of cortical bone.<sup>25</sup> The origin of the lack of collagen banding in micropores is unknown.

Ideally, scaffolds for bone regeneration should be comprised of resorbable materials, those that naturally dissolve and are replaced by bone growth.<sup>3</sup> Evidence of the initiation of resorption is seen in HA samples implanted for 7 months. The rough interface and lack of interfacial layer in areas along the interface are key features of enhanced biocompatibility and integration. In addition, the apparent resorption of apatite layer and direct growth of bone into the scaffold appears most

prominent in regions adjacent to grain boundaries, as demonstrated in Figure 6. This may be caused by the increased dissolution rate of HA at grain boundaries.

## CONCLUSIONS

The performance of bone regenerative scaffolds depends strongly on interfacial interactions. Synthetic HA and ZrO<sub>2</sub> scaffolds, produced with interconnected macro- and microporosity by free-form fabrication, were evaluated in the human maxilla. Sample preparation using the FIB technique enabled the investigation of the nanometer-scaled region at the scaffold-tissue interface. Scanning TEM revealed the development of an interfacial apatite layer on HA scaffolds *in vivo*, confirming the formation of bioactive fixation. A concentration gradient exists across this interfacial layer, suggestive of its development by a dissolution–reprecipitation mechanism. Indications of resorption were noted with increasing implantation time. In addition, extensive bone growth into microporosities indicates the great potential of HA scaffolds as a bone regenerative material. ZrO<sub>2</sub> scaffolds, however, showed a direct contact to bone in the absence of an interfacial apatite layer. As scaffold

geometry and pore size, morphology and volume were identical, the differences in *in vivo* response can be attributed to the material chemistry.

## ACKNOWLEDGMENTS

This study was made possible by the support of the VINNOVA VinnVäxt Program, Biomedical Development in Western Sweden, the Institute for Biomaterials and Cell Therapy, the Swedish Research Council (grant K2006-73X-09495-16-3), the Hjalmar Svensson Foundation, and the Canadian Centre for Electron Microscopy. The authors would like to thank Julia Huang and Carmen Andrei for their assistance with FIB and TEM.

## REFERENCES

1. LeGeros RZ. Properties of osteoconductive biomaterials: calcium phosphates. *Clin Orthop Relat Res* 2002; 395:81–98.
2. LeGeros RZ. Calcium phosphate-based osteoinductive materials. *Chem Rev* 2008; 108:4742–4753.
3. Hench LL. Biomaterials: a forecast for the future. *Biomaterials* 1998; 19:1419–1423.
4. Ducheyne P, Qiu Q. Bioactive ceramics: the effect of surface reactivity on bone formation and bone cell function. *Biomaterials* 1999; 20:2287–2303.
5. Sennerby L, Dasmah A, Larsson B, Iverhed M. Bone tissue responses to surface-modified zirconia implants: a histomorphometric and removal torque study in the rabbit. *Clin Implant Dent Relat Res* 2005; 7:s13–s20.
6. Malmström J, Adolfsson E, Jarmar T, Engqvist H, Thomsen P. Structure of the interface between bone and scaffolds of zirconia and hydroxyapatite. PhD thesis, Gothenburg University, 2007.
7. Jones AC, Arns CH, Huttmacher DW, Milthorpe BK, Sheppard AP, Knackstedt MA. The correlation of pore morphology, interconnectivity and physical properties of 3D ceramic scaffolds with bone ingrowth. *Biomaterials* 2009; 30:1440–1451.
8. Uchida A, Nade S, McCartney E, Ching W. Bone ingrowth into three different porous ceramics implanted into the tibia of rats and rabbits. *J Orthop Res* 1985; 3:65–77.
9. Shimazaki K, Mooney V. Comparative study of porous hydroxyapatite and tricalcium phosphate as bone substitute. *J Orthop Res* 1985; 3:301–310.
10. Bignon A, Chouteau J, Chevalier J, et al. Effect of micro- and macroporosity of bone substitutes on their mechanical properties and cellular response. *J Mater Sci Mater Med* 2003; 14:1089–1097.
11. Rusu VM, Ng C-H, Wilke M, Tiersch B, Fratzl P, Peter MG. Size-controlled hydroxyapatite nanoparticles as self-organized organic-inorganic composite materials. *Biomaterials* 2005; 26:5414–5426.
12. Giannuzzi LA, Stevie FA. A review of focused ion beam milling techniques for TEM specimen preparation. *Micron* 1999; 30:197–204.
13. Giannuzzi LA, Stevie FA. Introduction to focused ion beams. New York: SpringerLink, 2005.
14. Malmström J, Adolfsson E, Arvidsson A, Thomsen P. Bone response inside free-form fabricated macroporous hydroxyapatite scaffolds with and without an open microporosity. *Clin Implant Dent Relat Res* 2007; 9:79–88.
15. Donath K, Breuner G. A method for the study of undecalcified bones and teeth with attached soft tissues\*. *J Oral Pathol Med* 1982; 11:318–326.
16. Jarmar T, Palmquist A, Brånemark R, Hermansson L, Engqvist H, Thomsen P. Technique for preparation and characterization in cross-section of oral titanium implant surfaces using focused ion beam and transmission electron microscopy. *J Biomed Mater Res* 2008; 87A:1003–1009.
17. Williams DB, Carter CB. Transmission electron microscopy: a textbook for materials science. New York: Plenum Press, 1996.
18. Malmström J, Slotte C, Adolfsson E, Norderyd O, Thomsen P. Bone response to free form-fabricated hydroxyapatite and zirconia scaffolds: a histological study in the human maxilla. *Clin Oral Implants Res* 2009; 20:379–385.
19. Giannuzzi LA, Phifer D, Giannuzzi NJ, Capuano MJ. Two-dimensional and 3-dimensional analysis of bone/dental implant interfaces with the use of focused ion beam and electron microscopy. *J Oral Maxillofac Surg* 2007; 65:737–747.
20. Jantou V, Turmaine M, West GD, Horton MA, McComb DW. Focused ion beam milling and ultramicrotomy of mineralised ivory dentine for analytical transmission electron microscopy. *Micron* 2009; 40:495–501.
21. de Bruijn JD, van Blitterswijk CA, Davies JE. Initial bone matrix formation at the hydroxyapatite interface *in vivo*. *J Biomed Mater Res* 1995; 29:89–99.
22. Porter AE, Hobbs LW, Rosen VB, Spector M. The ultrastructure of the plasma-sprayed hydroxyapatite–bone interface predisposing to bone bonding. *Biomaterials* 2002; 23:725–733.
23. Akagawa Y, Ichikawa Y, Nikai H, Tsuru H. Interface histology of unloaded and early loaded partially stabilized zirconia endosseous implant in initial bone healing. *J Prosthet Dent* 1999; 69:599–604.
24. Hing KA, Annaz B, Saeed S, Revell PA, Buckland T. Microporosity enhances bioactivity of synthetic bone graft substitutes. *J Mater Sci Mater Med* 2005; 16:467–475.
25. Hodge AJ, Petruska JA. Recent studies with the electron microscope on ordered aggregates of the tropocollagen macromolecule. In: Ramachandran GN, ed. Aspects of protein structure. New York: Academic Press, 1963:289–300.

Copyright of Clinical Implant Dentistry & Related Research is the property of Wiley-Blackwell and its content may not be copied or emailed to multiple sites or posted to a listserv without the copyright holder's express written permission. However, users may print, download, or email articles for individual use.